

HOSTED BY



ELSEVIER

Contents lists available at ScienceDirect

Saudi Journal of Biological Sciences

journal homepage: www.sciencedirect.com

Original article

Synthesis and characterization of different complexes derived from Schiff base and evaluation as a potential anticancer, antimicrobial, and insecticide agent

Lotfi M. Aroua^a, Sadeq K. Alhag^b, Laila A. Al-Shuraym^c, Sabri Messaoudi^d, Jazem A. Mahyoub^e,
Mohammad Y. Alfaifi^f, Wafa Mohammed Al-Otaibi^{g,*}^a Department of Chemistry, College of Science, Qassim University, Buraydah, Qassim, Saudi Arabia^b Biology Department, College of Science and Arts, King Khalid University, Muhayl Asser, Saudi Arabia^c Biology Department, Faculty of Science, Princess Nourah Bint Abdulrahman University, Riyadh, Saudi Arabia^d Department of Chemistry, College of Science, Qassim University, Buraydah, Qassim, Saudi Arabia^e Biology Department, College of Science, King Abdulaziz University, Jeddah, Saudi Arabia^f Biology Department, College of Science, King Khalid University, Abha, Saudi Arabia^g Department of Biology, College of Science, Taif University, Taif, Saudi Arabia

ARTICLE INFO

Article history:

Received 12 December 2022

Revised 23 January 2023

Accepted 8 February 2023

Available online 14 February 2023

Keywords:

2-aminomethyl benzimidazole

Schiff base complex

2-hydroxynaphthaldehyde

Potential anticancer agents

Antimicrobial agents

Insecticide agents

ABSTRACT

The condensation of (1H-benzimidazole-2-yl) methanamine, with 2-hydroxy naphthaldehyde lead to Schiff base ligand (H2L) (1). This was later reacted with metal salts (ZnCl₂, CrCl₃·6H₂O, and MnCl₂·4H₂O) to afford the corresponding metal complexes. Biological activity findings indicate that the metal complexes have promising activity against *Escherichia coli* and *Bacillus subtilis* and modest activity against *Aspergillus niger*. The in vitro anticancer activities of Zn (II), Cr (III), and Mn (II) complexes were investigated and the best results were observed with Mn (II) complex as the most potent cytotoxic agent toward human cell lines colorectal adenocarcinoma HCT 116, hepatocellular carcinoma HepG₂ and breast adenocarcinoma MCF-7 with 0.7, 1.1 and 6.7 μg of inhibitory concentration IC₅₀ values respectively. Consequently, the Mn (II) complex and ligand were docked inside the energetic site of ERK2 and exhibited favorable energy for binding. The investigation of biological tests towards mosquito larvae indicates that Cr (III) and Mn (II) complexes manifest strong toxicity against *Aedes aegypti* larvae with 3.458 and 4.764 ppm values of lethal concentration LC₅₀, respectively.

© 2023 The Author(s). Published by Elsevier B.V. on behalf of King Saud University. This is an open access article under the CC BY-NC-ND license (<http://creativecommons.org/licenses/by-nc-nd/4.0/>).

1. Introduction

Benzimidazole system emerged as a targeted potent class of heterocyclic compounds in the development of drugs with various activities against multiple diseases, covering antibacterial, anti-tuberculosis, antimalarial, antihistamine antifungal analgesic, and

anti-inflammatory, and anti-amoebic, insecticidal activity, and anti-ulcer (Sondhi et al,2006; Wang et al, 2012; Ganie et al., 2019; Dokla et al, 2020; Cheddie et al, 2020; Patel et al, 2020; Huszar et al, 2020). Recently, the benzimidazole nucleus is currently used as a precursor to developing multiple compounds owing to their different pharmaceutical applications as antihypertensive and antiallergic agents (Narasimhan et al., 2012; Zhou & Huang, 2020).

In addition, many reviews reported the bioactive efficiency of benzimidazole scaffolds against hepatitis disease and are considered a new class of inhibitors of hepatitis B and C virus (Li et al., 2007; Alorini et al., 2022). As a consequence, diverse drugs elaborated from benzimidazole have been introduced into the market including albendazole (antimicrobial), omeprazole (anti-ulcer), Bendamustine (anti-tumor), Enviradene (anti-viral), Candesartan (anti-hypertensive), and Benoxapofen analog (anti-inflammatory) (Bansal & Silakari, 2012). On the other hand, multiple reports

* Corresponding author.

E-mail addresses: lm.aroua@qu.edu.sa (L.M. Aroua), salhag@kku.edu.sa (S.K. Alhag), laalshuraym@pnu.edu.sa (L.A. Al-Shuraym), S.Messaoudi@qu.edu.sa (S. Messaoudi), jabdulrahman@kau.edu.sa (J.A. Mahyoub), alfaiifi@kku.edu (M.Y. Alfaifi), w.alotaibi@tu.edu.sa (W.M. Al-Otaibi).

Peer review under responsibility of King Saud University.



Production and hosting by Elsevier

<https://doi.org/10.1016/j.sjbs.2023.103598>

1319-562X/© 2023 The Author(s). Published by Elsevier B.V. on behalf of King Saud University.

This is an open access article under the CC BY-NC-ND license (<http://creativecommons.org/licenses/by-nc-nd/4.0/>).

described the benzimidazole nucleus as an anti-tumor and anti-cancer agent (Djemoui et al., 2020). According to the Abdelgawad et al., (2017) the synthesis of benzimidazole derivatives incorporating a pyrazole moiety and approved a considerable potential as anti-proliferative activity toward non-small cell lung cancer (A 549) cell lines and breast adenocarcinoma (MCF-7) Abdelgawad et al., 2017). Certain benzimidazole cores have multiple applications, in particular, currently used as ligands in metal complexes preparation. Several benzimidazole complexes were examined and exhibited diverse biological activity including antiproliferative, antimicrobial, antitumor, antimalarial, and anticancer activity (Welsh et al., 2020). Yılmaz & Kuçukbay (2020) described the synthesis and anticancer assessment target benzimidazole complexes of Co (II) and Zn (II) on tumor cell lines DU-145 and A- 2780.

Moreover, complexes generated from 2-aminomethyl benzimidazole are well documented and manifested excellent bioactivities in the medical and pharmaceutical fields (Abdelkarim et al., 2015). Several reviews suggested the potency of 2-aminomethyl benzimidazole complexes toward cancer cells notably cytotoxic action on the cell line of breast adenocarcinoma MCF-7, carcinoma of the colon (HCT116), carcinoma of larynx (HEP2), neuroblastoma (SHSY5Y), and carcinoma of hepatocellular (HepG2) (El-Sherif, 2011; Cavicchioli et al., 2019). Naeema et al., (2017) research team explained only the combination of metal complexes using metal salt $\text{CoCl}_2 \cdot 6\text{H}_2\text{O}$, $\text{NiCl}_2 \cdot 6\text{H}_2\text{O}$, $\text{CuCl}_2 \cdot 2\text{H}_2\text{O}$, and $\text{Zn}(\text{CH}_3\text{COO})_2 \cdot 2\text{H}_2\text{O}$ and ligand prepared by condensing 2-aminomethylbenzimidazole and 2-hydroxy naphthaldehyde (Naeema et al., 2017).

In continuation elaborate and discovered a novel target compound possessing biological activities (Al-Hakimi et al., 2020). we described the combination and characterization of novel metal complexes derived from Schiff base as ligand and ZnCl_2 , $\text{CrCl}_3 \cdot 6\text{H}_2\text{O}$, and $\text{MnCl}_2 \cdot 4\text{H}_2\text{O}$ as metal salts. The objective of this work is to elucidate the bioactivities properties of Schiff base complexes. The evaluation as potential anticancer cell, antibacterial, antifungal, and insecticide agents of complexes was investigated.

2. Materials and methods

Between 400 and 4000 cm^{-1} , an FT-IR Spectrometer Carry 600 was used with a microscope to capture FT-IR spectra. The Shimadzu DTG-60 was used for thermal analysis using TGA and DTA. The average sample weight for DTA measurements was 10 mg Al_2O_3 . DMF was used to record the electronic absorption spectra from a UV-2102 Shimadzu instrument. Sigma-Aldrich provided the methanamine. High-resolution mass spectra (EI- HRMS) were created using the JEOL AccuTOF LC-Plus mass spectrometer. DART-TOF-MS was employed in positive mode to record the mass spectra of the complex. ^1H NMR and ^{13}C NMR spectra were obtained on a Bruker NMR, using 400 MHz and 100 MHz, respectively. The solvent was DMSO d_6 and tetramethylsilane (TMS) was the internal standard reference.

2.1. Preparation of ligand (HL) (1)

This protocol was developed using the available literature (Naeema et al., 2017). Using a solution of 2-(1H-benzimidazole-2-yl)methanamine (1.47 g, 10 mmol) in 35 mL of anhydrous ethanol, it was gradually heated to 65 °C for 30 min. The naphthaldehyde solution (1.72 g, 10 mM) was then dissolved in 20 mL of anhydrous ethanol while the combination was stirred for another four hours. After that, the solute was separated from the solvent by relieving pressure. The remains were filtered ether washed, and ethanol recrystallization. The reported data were agreed upon and described.

75 % yield. IR (KBr, cm^{-1}): 3420, 3255, 1631, 1548, and 1320 cm^{-1} . 420, 318, and 272 nm for UV-vis. m.p.126 °C yield, m.p. 301 m/z for EI-MS (DMF, maximum). δ ppm 4.07 (2H, s, CH_2), 9.29 (1H, s, N = CH), 6.77–8.09 (10H, d, m, Ar-H), 14.16 (1H, d, ArOH), 12.66 (1H, s, NH imidazole), and 5.29 (1H, s, N = CH) ppm were discovered in the ^1H NMR (400 MHz, DMSO d_6) experiment. It was possible to obtain the following ^{13}C NMR (100 MHz, DMSO d_6) values: δ ppm: 50.09, 106.99, 112.02, 119.03, 119.25, 123.39, 124.57, 126.3, 128.76, 129.48, 134.17, 134.61, 138.01, 151.06, 161.46, and 175.68 ppm.

2.2. Preparation of metal complexes

The ligand (5 mmol) was thawed in 20 mL of hot ethanol. The amounts of the metal salts ZnCl_2 , $\text{CrCl}_3 \cdot 6\text{H}_2\text{O}$, and $\text{MnCl}_2 \cdot 4\text{H}_2\text{O}$ in this solution were 5 mmol each. The reaction mixture was gradually heated before being refluxed for three hours. After cooling, the produced liquid was combined with 20 mL of ethanol and then filtered. After collecting the unwashed crude precipitate, hot ethanol (2x10 mL) and ether (2x20 mL) washes were performed, and the mixture was vacuum-dried over anhydrous CaCl_2 .

Cr (III) complex: 82 % yield, Dark Brown precipitate, m.p. > 30 0 °C, UV-vis (DMF, max): 282, 390, 440, and 510 nm. EI-HRMS (DART-TOF-MS) m/z = 386.22754, 341.20671, 314.13429, 261.10427, 215.12690, 186.08176, 124.04395, 108.02147. IR (KBr.): 3420, 3250, 1615, 1560, 1330, 680, 555, 420 cm^{-1} . Elements examined: Calculated for $\text{C}_{19}\text{H}_{16}\text{Cl}_2\text{CrN}_3\text{O}_2$: C, 51.72, H, 3.66, and N, 9.52. Found: C, 51.52, H, 3.56, and N, 9.64.

Mn(II) complex: Pink precipitate with a 75 % yield, mp of 270 °C, and UV-vis (DMF, max) of 282, 500, 620, and 710 nm. HRMS (DART-TOF-MS) m/z = 380.27609, 324.22166, 289.14011, 261.10460, 226.18776, 180.14152, 133.06316, 102.06690. IR (KBr.): 3430, 3251, 1620, 1550, 1325, 685, 560, 415 cm^{-1} . Elements examined: Calculated for $\text{C}_{19}\text{H}_{18}\text{ClMnN}_3\text{O}_3$: C, 53.47; H, 4.25; N, 9.85. Found: C, 53.27; H, 4.13; N, 9.72.

Zn(II) complex: 75 % yield, Orange precipitate; mp: 195 °C, UV-vis (DMF, λ^{max}): 280 nm. IR (KBr) ν : 3425, 3260, 1625, 1560, 1325, 660, 590, 590 cm^{-1} . HRMS (DART-TOF-MS) m/z = 455.30303, 452.99893, 377.27386, 336.22481, 296.19970, 250.13073, 189.13762. Elemental Analysis: Found: C, 49.88; H, 3.65; Cl, 15.56; N, 9.11. Calculated for $\text{C}_{19}\text{H}_{17}\text{Cl}_2\text{N}_3\text{O}_2$ Zn: C, 50.08; H, 3.76; Cl, 15.56; N, 9.22.

2.3. The culture of cells

Type of American Culture Collection (ATCC) supplied breast adenocarcinoma cell line (MCF-7) and colorectal adenocarcinoma cells. We used RPMI – 1640 with 10 %v/v bovine fetal serum, 100 units/mL penicillin, and 5 % CO_2 at 37 °C for cells culture in humidified air (Mahmoud et al., 2012; Ibrahim et al., 2016).

2.4. Cytotoxicity test

Sulforhodamine B (SRB) test was used to assess the ligand's and its complex are in vitro cytotoxic activity against the human colon cancer cell line HCT 116, the breast adenocarcinoma cell line MCF-7, and the human liver cancer cell line HepG2. Six concentrations (0.01, 0.1, 1, 10, 100, and 1000 μg) of each complex were used to treat various cell types, with untreated cells acting as controls. All cells were exposed to TCA (10 %w/v) for an hour at 4 °C after being cultured with each dose for 72 h. The cells were carefully washed before being stained for 10 min in the dark with a 0.4 % (w / v) SRB solution. A 1 % (v / v) glacial acetic acid solution was applied to remove extra stains.

Tris-HCl was then added after the SRB - stained cells had been dried overnight. A 540 nm microplate reader was used to measure

the color intensity after that. The relationship between the feasibility of each cancer cell line's viable cells and the chemical concentration was examined using SigmaPlot 12.0 software to determine the IC50 (Jang et al., 2002).

2.5. Molecular docking and computational details

To pinpoint the precise location of these substances in the receptor binding site, we used molecular docking to examine the interaction between the ligand and the ERK2 active site. The protein data bank was used to locate the crystal structure of ERK2 (PDB code: 5buj). The structure was cleared of the water molecules and the CO-crystallized ligand. Morris et al., 2008 created the PDBQT file after assigning the polar hydrogens and Gasteiger charges with the help of AutoDockTools1.5.2 (ADT) (2008). Using ADT, a docking grid was chosen. The grid (x, y, and z) has $25 \times 25 \times 25$ dimensions.

The docked molecules were first optimized using density functional theory by Frisch et al. (2013) utilizing the Gaussian 09 program and the B3LYP level of theory. We applied the basis set LANL2DZ to the Mn atom. Then, all additional atoms were subjected to the 6-31G(d) basis set. The ligand's HOMO and LUMO orbitals were both discernible at the same level. Using ADT, the PDB files were transformed into PDBQT. The Autodock vina software, which had an exhaustiveness parameter of 32, was used to do the docking computations (Trott & Olson, 2010). Discovery Studio Visualizer determined how the receptor and ligand interacted, and ADT confirmed the study (Biovia, 2015).

2.6. Antifungal and antimicrobial effect

The diffusion method was employed in the microbiology section to conduct these tests (Shakdofa et al., 2021). *Escherichia coli* and *Bacillus subtilis* were used to test the antibacterial activity. *Aspergillus niger*, a kind of antifungal, was used to test the antifungal activity of the DMSO solution. As a control, a poured disc that was empty was employed. For the 10^{-3} M compounds that were examined, the resultant hole sites were observed. It was determined to what extent the chemical solutions inhibited the microbes. Tetracycline and nystatin were utilized as antibacterial and antifungal positive controls, respectively, to compare inhibition. The bacterial and fungal growth inhibitions were measured in the millimeter-sized regions surrounding the holes.

2.7. Mosquitoes rearing

At the Dengue mosquito station in Jeddah, the breeding of mosquitoes (*Aedes aegypti*) was done in the southern part of the house. The produced mosquito larvae were placed in plastic trays painted with enamel and filled with tap water for rearing. In each case, the growing environment was set at $(27 \pm 2 \text{ }^\circ\text{C})$ and 74–77 % RH with light time (10:14 dark and light). The mosquitoes were raised for three generations and fed a special diet (Collee et al., 1997; Algamdi and Mahyoub 2022).

2.8. The activity of larvicidal

The Larval susceptibility test was conducted according to the method of (Mahyoub, 2019). Treatments were carried out by exposing early 4th instar larvae of *Ae. aegypti* to various concentrations of the tested compounds in groups of glass beakers containing 100 mL of tap water. Five replicates of 20 Larvae each per concentration, and so for control trials were set up. The Larvae were given the usual larval food during the experiments. The percentage of Mortalities of larvae was recorded and compared with

those of the controls under the same conditions of tests (Rahuman et al., 2000; Hayat et al., 2022).

3. Results

3.1. Chemistry

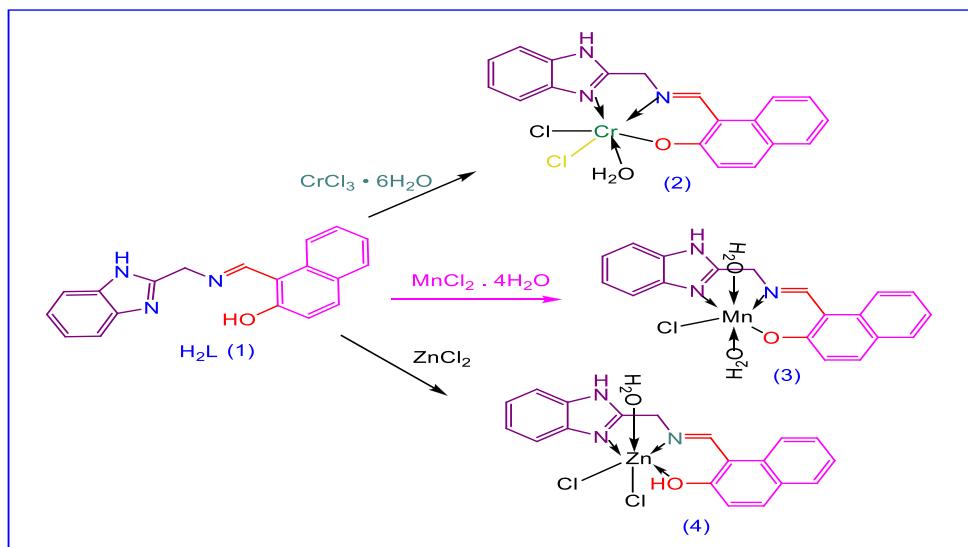
The ligand reaction between 2-aminomethyl benzimidazole and 2-hydroxynaphthaldehyde was prepared using ethanol as the solvent. Complexes were made by mixing one equivalent of a ligand (HL) with one equivalent of each metal salt (ZnCl_2 , CrCl_3 , and $\text{MnCl}_2 \cdot 4\text{H}_2\text{O}$) in a pot of boiling ethanol (Scheme 1). The new complexes were identified using high-resolution mass spectrometry (EI-HRMS), UV-Visible, FT-IR, and thermal analyses.

3.2. High-resolution mass spectra

The lack of a molecular peak was evident in the mass spectra of the Cr (III) complex shown in Fig. 1. In essence, the molecular ion peak at $m/z = 386.22754$ which corresponds to the loss of the chlorine atom and the water molecule served as evidence for the structure (calcd. 386.01523). A link between 2-aminoethyliminomethylphenol and chromium metal is indicated by the basic component at $m/z = 215.12690$ (calcd. 215.02765). Additionally, the spectra show that N-(2-hydroxybenzylidene) methanaminium connected to chromium has another value of peak at $m/z = 186.08176$ (calcd. 186.00055). The peak at $m/z = 108.02147$ that the o-phenyl diamine produced (calcd. 108.06875). The chromium was connected to the ligand by an oxygen atom and two chlorine atoms, as these results further confirm. The chromium metal coordination was established with both the azomethine group of ligand and water molecules (Scheme 1).

The molecular ion peak absence can be seen in the mass spectra of the Mn (II) complex shown in Fig. 2. The fragment at $m/z = 380,27609$ (calculated as 380,03569) agrees with benzoimidazolmethyliminomethyl-3-methyl-4-vinyl-phenol joined with manganese and a chlorine atom, providing further structural confirmation. The manganese-related compound benzimidazolmethyliminomethyl-3-methyl-cyclohexanol is responsible for the observed peak at $m/z = 324.22166$ (calcd. 324.09086). Benzo-imidazole methyl phenyl methenamine joined to manganese is the component at $m/z = 289.14011$ (calcd. 289.04062). Hexane-3-aminium is connected to the fundamental fragment at $m/z = 102,0.6690$ (calcd. The octahedral structure of the complex was formed and assumed, according to these data. A chlorine atom and a hydroxyl group connect the manganese to the ligand. The coordination of the manganese has been provided by both azomethine groups and two water molecules (Scheme 1).

The molecular ion peak M^+ at $m/z = 452,99893$ and $[\text{M}^{2+}]^+$ at $m/z = 455.30303$ (calcd. 455,01403), corresponding to chlorine isotope, are present in the mass spectra of the Zn(II) complex shown in Fig. 3. This suggests octahedral coordination with the ligand, two chlorine atoms, and one water molecule. The component at $m/z = 377,27386$ (calcd. 377,02734) shows that zinc and chlorine are linked with benzoimidazolmethyliminomethyl-3,4-dimethyl phenol. The peak at $m/z = 336,22481$ (calcd. 336,00079) indicates that zinc and chlorine atoms are linked to phenylamino methyl imino methyl phenol. The benzo imidazole ethanamine motif linked to zinc, chlorine, and water molecules is attributed to the peak at $m/z = 296,19970$ (calcd. 295,93359). The fundamental fragment at $m/z = 189,13762$ (calcd. 189,02444), which corresponds to 4,5-dimethyl-4,5-dihydroimidazolmethaniminium linked with zinc, further supports the confirmation of its structure. This erudition, in the zinc complex case, asserts the metal is coordinated first to the ligand by both the azomethine group and hydroxyl group sec-



Scheme 1. Structures of Cr (III), Mn (II), and Zn (II) complexes.

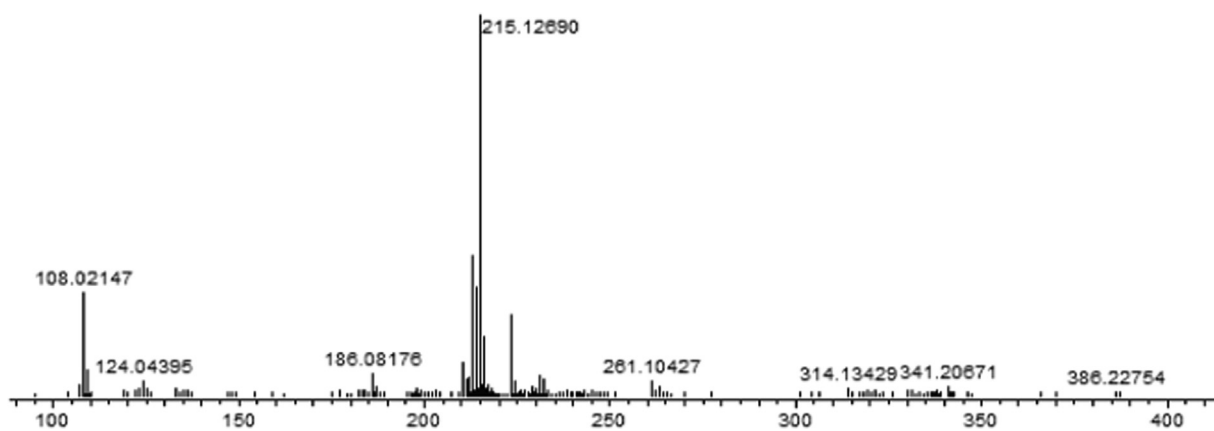


Fig. 1. Cr (III) complex mass Spectra.

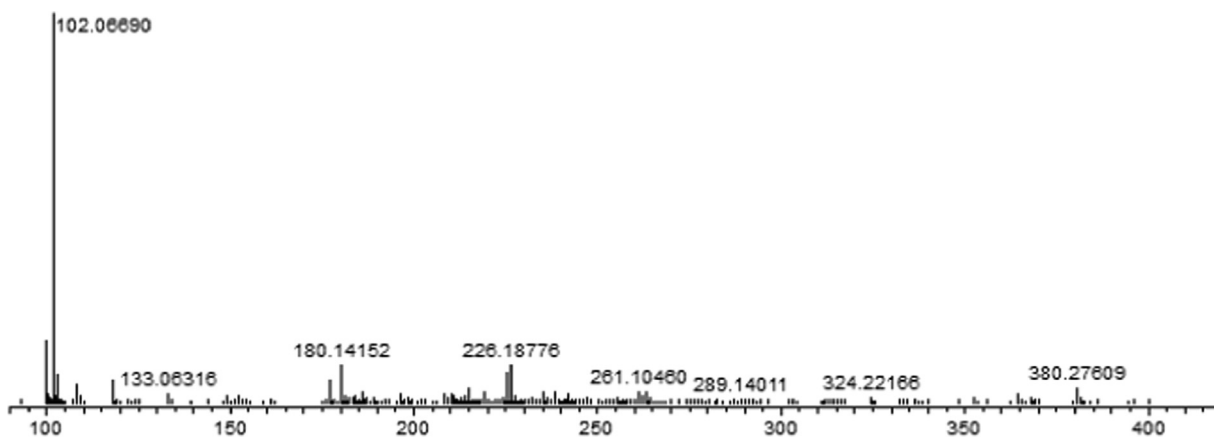


Fig. 2. Mn (II) complex mass spectra.

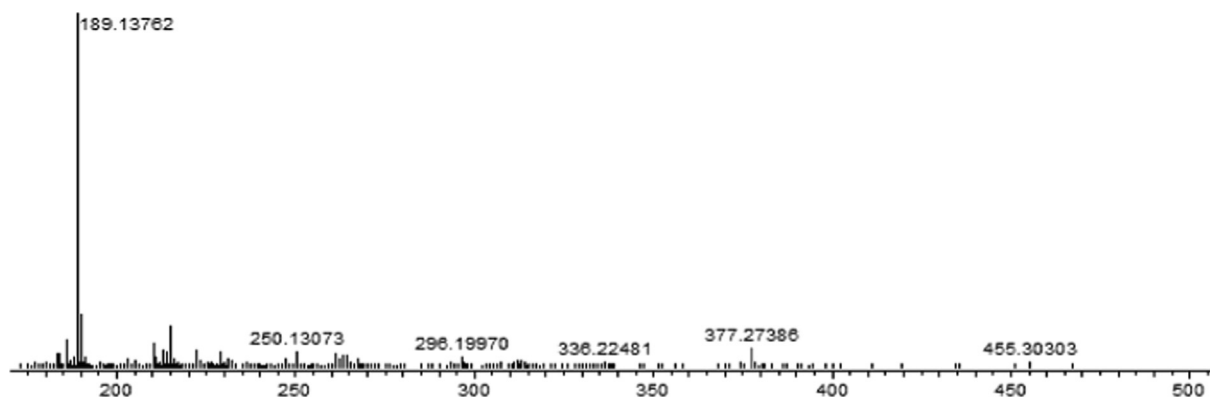


Fig. 3. Zn (II) complex mass spectra.

ond with one water molecule and connected with two chlorine atoms.

3.3. Electronic spectra

The prepared compounds had trouble dissolving completely in ethanol and methanol, so the Ultraviolet–visible absorption of all the compounds was examined in DMF at room temperature. The outcomes were summarized in Table 1. The ligand (HL) has three different types of electron transitions, and the first one, which occurs at 272 nm, is in the $\pi \rightarrow \pi^*$ band. The second transition, which is associated with the $n \rightarrow \pi^*$ band, takes place at 318 nm. While the third transition, which has the transition type $(2) 3A_2 g(F)3T_1 g$, appears at 420 nm (F). Theoretical calculations revealed that the energy variation among the highest occupied molecular orbital and lowest unoccupied molecular orbital was 3.96 eV. (Fig. 4a, Fig. 4b, and Fig. 4c). In this instance, the power and stabilization of complexes and the bonds that make up those complexes are predicted using the energy difference between these two boundary orbitals. The compound is stabilized by the arrangement of the single and double bonds, as well as by the free electrons, which also serves to increase the compound's chemical reactivity. A high electron density in the ligand results in efficiency and extremely high activity.

3.4. Infrared spectra

There are three possible locations for the ligand to bind to the metal ion. These three sites are the hydroxyl group's oxygen, the benzimidazole compound's nitrogen atom, and the azomethine ($-C=N-$) compound's nitrogen atom. As a result, the ligand exhibits neutral, monobasic, ionic, or nonionic tridentate behavior. The

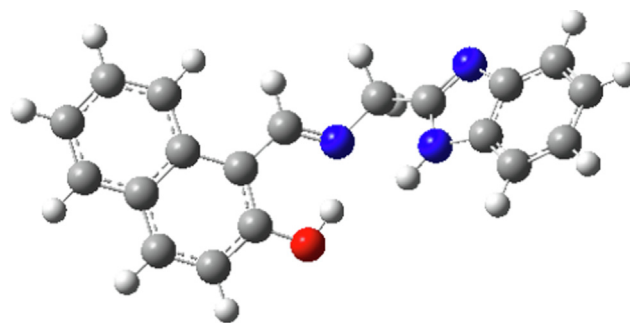
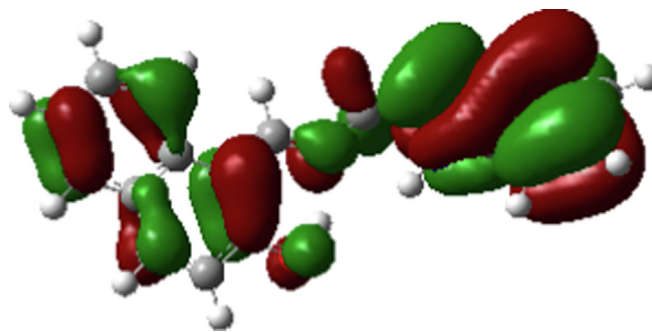
Fig. 4a. Spatial representation of Ligand H₂L(1).

Fig. 4b. HOMO of the ligand.

Table 1
ligand and the metal complexes (Analytical and electronic data).

Compound	Colour	Yield (%)	Mp(°C)	λ^{\max} (nm)	ϵ (mol ⁻¹ cm ⁻¹)	Assignment
C ₁₉ H ₁₅ ON ₃ (1)	Yellow	80	126	272	7.7 X10 ⁻³	$\pi \rightarrow \pi^*$
				318	2.5 X10 ⁻³	$n \rightarrow \pi^*$
				420	4.1 X10 ⁻⁴	$(\nu_2) 3A_2 g(F) \rightarrow 3T_1 g(F)$
C ₁₉ H ₁₆ O ₂ N ₃ Cl ₂ Cr (2)	brown	82	300	282	2.5 X10 ⁻³	$\pi \rightarrow \pi^*$
				390	3.2 X10 ⁻⁴	$4A_2 g(F) \rightarrow 4T_1 g(P)$
				440	1.8 X10 ⁻⁴	$4A_2 g(F) \rightarrow 4T_1 g(F)$
				510	3.1 X10 ⁻⁴	$4A_2 g(F) \rightarrow 4T_2 g(F)$
				500	5.3 X10 ⁻³	$\pi \rightarrow \pi^*$
C ₁₉ H ₁₈ O ₃ N ₃ ClMn (3)	pink	75	270	282	5.3 X10 ⁻³	$\pi \rightarrow \pi^*$
				620	3.6 X10 ⁻⁴	$6A_1 g \rightarrow 4Eg(4G)$
				620	2.2 X10 ⁻⁴	$6A_1 g \rightarrow 4T_1 g(4G)$
C ₁₉ H ₁₇ O ₂ N ₃ Cl ₂ Zn (4)	Orange	75	195	710	1.3 X10 ⁻⁴	$6A_1 g \rightarrow 4Eg(4D)$
				710	1.3 X10 ⁻⁴	$6A_1 g \rightarrow 4T_1 g(4p)$
				280	5.2 X10 ⁻³	$\pi \rightarrow \pi^*$

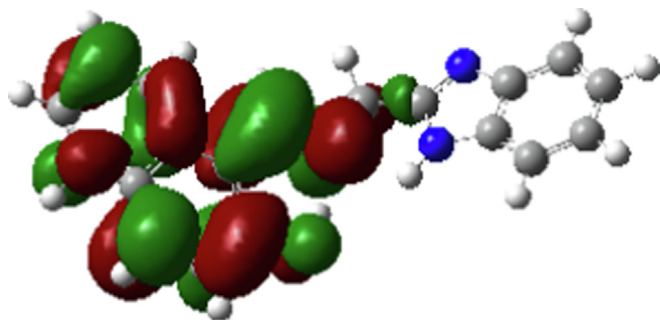


Fig. 4c. LUMO of the ligand.

ligand (HL) behaves as a monobasic tridentate chelator in the metal complexes (2) and (3), forming two succeeding cycles of 6 and 5. This conduct was demonstrated through the benzimidazole ring's negative shift in status as well as the absence of the hydroxyl group's absorption summit. When metal is present, it forms six and five rings while the ligand serves as an inactive tridentate. This is demonstrated by the hydroxyl group, benzimidazole ring, and azomethine group all changing negatively in their locations.

The phenolic hydroxyl group's vibration and stretching caused the ligand to have substantial and powerful features at 3420 cm^{-1} , as seen in Table 2. The metal complexes (2) and (3), on the other hand, exhibit the loss of the hydroxyl group stretching vibration due to removal group of the hydroxyl during the production methods. The broad medium band at 3255 cm^{-1} is produced by the (NH) group (Table 2).

The absorption of the stretching vibration of the phenolic hydroxyl group coupled to the Zn (II) ion allows for the definitive identification of the medium band at 3440 cm^{-1} in the metal complex (4). The spectra of this metal combination show coordinated nitrogen absorption in the benzimidazole ring and azomethine group at 3260 cm^{-1} and 1620 cm^{-1} , respectively. Additional proof for the coordinate was provided by the presence of bands at 660 cm^{-1} , 590 cm^{-1} , and 402 cm^{-1} , which correspond to $\nu(\text{OM})$, (NM), and (CIM), respectively.

3.5. Thermal analysis

The complexes (2), (3), and (4)'s thermal analyses of metal complexes (DTA and TGA curves) at the temperature range ($27\text{--}550\text{ }^\circ\text{C}$) (4). It has been determined that these metal complexes are extremely thermally stable up to $120\text{ }^\circ\text{C}$. The thermal spectra also showed a loss of strongly coordinated water molecules between 230 and $270\text{ }^\circ\text{C}$. The disintegration of complex (2) peaked at temperatures of $130\text{ }^\circ\text{C}$ with a loss of weight 4.05% (calculated as 4.08%), matching the loss of one coordinated water molecule, and at ($250\text{--}260\text{ }^\circ\text{C}$) with a mass consequence loss of one chlorine molecule at a rate of 16.70% (calculated as 16.77%), matching the loss of chlorine molecule. Finally, the thermal spectra of complex (2) showed a peak at $560\text{ }^\circ\text{C}$ with a weight decrease of 43.10% (calculated as 43.14%), suggesting the formation of Cr_2O_3 . Between

150 and $170\text{ }^\circ\text{C}$, the metal complex (3) displays an endothermic peak in addition to a peak of decomposition with a weight loss of 8.35% (calculated at 8.43%) that corresponds with the loss of two coordinated water molecules. The spectra also showed an endothermic summit with a weight loss of 9.30% (calculated as 9.33%) at $250\text{ }^\circ\text{C}$, which corresponds to the loss of one hydrochloride molecule. Further evidence for the formation of MnO_2 includes the clear peak at $540\text{ }^\circ\text{C}$ and a weight loss rate of 24.45% (calculated at 24.53%).

With a weight loss of 3.85% (calculated as 3.95%) and a temperature of $170\text{ }^\circ\text{C}$, the zinc complex (4) started to disintegrate. This is because one coordinated water molecule was missing. The zinc complex, on the other hand, displayed a weight loss of 16.10% (calculated at 16.22%) and a peak in its spectra at $250\text{ }^\circ\text{C}$, which is caused by the removal of one chlorine molecule. Also indicating the formation of ZnO is the distinctive peak at $535\text{ }^\circ\text{C}$ with a weight loss of 21.90% (calculated at 22.19%).

3.6. anti-tumor activities in vitro

The SRB assay was used to examine the metal complexes' in vitro cytotoxic effects on the HepG2 and HCT 116 over the concentration range of 0.01 to $1000\text{ }\mu\text{g}$. The results of the different analyses are compiled in Fig. 5. On human solid tumor cell lines, the tested substances displayed the cytotoxic activity of varying degrees. With inhibitory concentration values of IC_{50} of 46.1 and 36.6 g , respectively, the chromium complex has a negligible toxic effect on HCT 116 and HepG2 tumor cells, according to Table 3. The same substance failed to have any cytotoxic activity against breast adenocarcinoma MCF-7 cells up to a concentration of 100 g . (Table 3).

The HCT 116 and HepG2 tumor cells were moderately toxic to the ligand and zinc complex, with IC_{50} values ranging from 10.2 g to 30.5 g and 1.6 g , respectively. The ligand also shows notable activity against hepatocellular carcinoma (HepG2), with an IC_{50} of $5.7\text{ }\mu\text{g}$ (Table 3). The manganese complex delivered the best outcomes because it has the most cytotoxic effects on HCT 116, MCF-7, and HepG2 cells, with IC_{50} values of 6.7 , 1.1 , and $0.7\text{ }\mu\text{g}$ respectively.

3.7. Docking study

Molecular docking was used to examine the inhibitory activity on ERK2 (PDB code: 5buj) and to display the modes of binding between our chosen compounds and the active site. For the chosen compounds, the ideal docking positions were found (Fig. 6). The Mn (II) complex with its fully formed first hydration sphere had a binding energy of $-9.1\text{ kcal mol}^{-1}$, while the ligand alone had a binding energy of $-9.5\text{ kcal mol}^{-1}$. These energies indicated that these compounds preferred to bind to the active site. The Mn (II) complex docking results give an energy of $-10.3\text{ kcal mol}^{-1}$ when two of its coordinated water molecules are absent. This stability indicates that these substances are strong inhibitors and fit the catalytic site's pocket perfectly. Since both the ligand and the Mn complex structures have high binding energies, the docking simu-

Table 2
IR spectral data of organic ligand and its metal complexes.

No.	Ligand/complexes	$\nu(\text{OH})/\text{H}_2\text{O}$	$\nu(\text{NH})$	$\nu(\text{C}=\text{N})$	$\nu(\text{C}-\text{O})_{\text{ph}}$	$\nu(\text{M}-\text{O})$	$\nu(\text{M}-\text{N})$	$\nu(\text{M}-\text{Cl})$
1	$\text{C}_{19}\text{H}_{15}\text{N}_3\text{O}$ (H ₂ L)	3420 sh	3255	1631, 1570	1320	–	–	–
2	$\text{C}_{19}\text{H}_{16}\text{O}_2\text{N}_3\text{Cl}_2\text{Cr}$	3420 br	3250	1615, 1560	1330	680	555	420
3	$\text{C}_{19}\text{H}_{18}\text{O}_3\text{N}_3\text{ClMn}$	3430 br	3251	1620, 1550	1325	685	560	415
4	$\text{C}_{19}\text{H}_{17}\text{O}_2\text{N}_3\text{Cl}_2\text{Zn}$	3425 (br)	3260	1625, 1560	1325	660	590	412

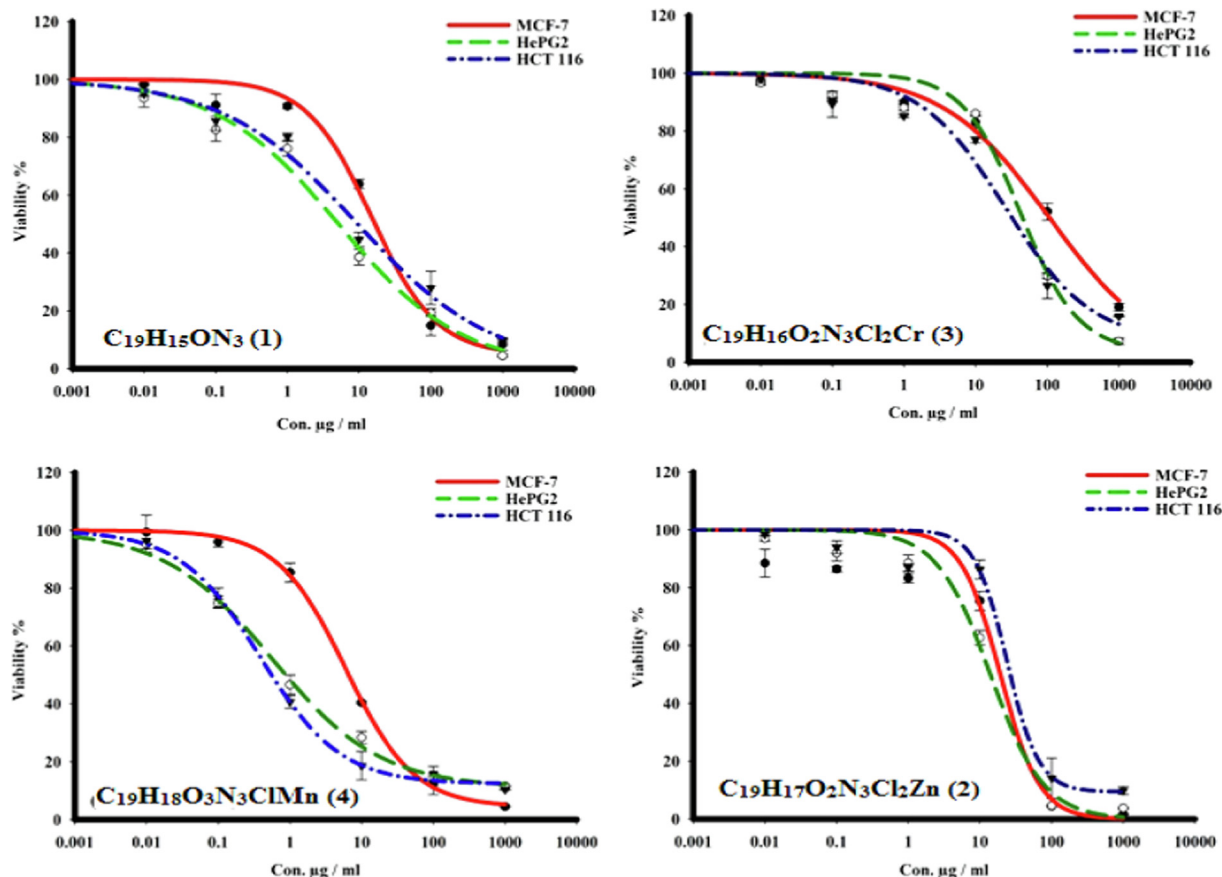


Fig. 5. Cell viability curves of MCF-7, HepG2, and HCT 116 cancer cell lines that were treated with ligand (H2L) and metal complexes with various concentrations for 72 h by SRB stain.

Table 3

The IC₅₀ of the ligand and its metal complexes against various cancer cell lines.

Compounds	IC ₅₀ (µg)		
	MCF-7	HepG2	HCT 116
C ₁₉ H ₁₅ N ₃ O	17.6 ± 1.5	5.7 ± 0.5	10.2 ± 1.3
C ₁₉ H ₁₆ O ₂ N ₃ Cl ₂ Cr	≥ 100	46.1 ± 1.6	36.6 ± 2.6
C ₁₉ H ₁₈ O ₃ N ₃ ClMn	6.7 ± 0.5	1.1 ± 0.2	0.7 ± 0.1
C ₁₉ H ₁₇ O ₂ N ₃ Cl ₂ Zn	19.5 ± 1.1	14.4 ± 0.5	30.5 ± 1.6

lation results are consistent with the IC₅₀ values against various tumor cell lines. According to docking studies (Fig. 7), the interaction of the ligand with the enzyme results in two hydrogen bonds (2.07 and 2.10) with Met 106 and one hydrogen bond (2.01) with LYS 112. In addition, several π -sigma interactions are found with VAL 37, LEU 154, and ILE 29, and there are also π -alkyl interactions with CYS 164, ALA 50, and LEU 105.

3.8. Antimicrobial and antifungal effect

In the microbiology lab, tests on the ligand and its metal complexes were conducted using the pathogenic bacteria *E. coli* and *B. subtilis* as well as the fungus *A. niger*. In varying degrees, each compound exhibited a clear and distinct activity against the bacteria and fungi. Comparing the obtained inhibition results to those for standard drug compounds used for the same purpose (Table 4 and Fig. 8). The ligand demonstrated high efficacy against both bacteria and fungi when compared to its metal complexes, outperforming in its outcome the action of the conventional drugs used,

which were used for a single purpose only. The reason for the increased activity of the ligand over its metallic complexes may be due to the ease of movement of electrons, which can be associated with the cell wall of bacteria or fungi.

3.9. Mosquito larvae bioassay

The larvicidal effects of the ligand H2L and the various compound during the exposure period on *Ae. aegypti* larvae are shown in Tables 5 and 6, respectively. The relationship between various concentrations of these compounds and larval mortality is shown in Fig. 9. When exposed for 48 h, the ligand H2L was more effective in causing larval death, reaching an average mortality rate of 99 % at a concentration of 10 ppm and 2.521 ppm values for the LC₅₀. Zinc (II) complex engender was a maximum of mortality within 48 h 73.5 % at a concentration of 10 ppm with 6.96 ppm values of lethal concentration LC₅₀. However, chromium (III) and manganese (II) complexes manifest an exciting increment of toxicity against *Ae. aegypti* larvae with 3.458 and 4.764 ppm values of LC₅₀ after 48 h of exposure, respectively.

4. Discussion

Due to the lanthanide complex binding statute, only 6 of the lanthanide (III) coordination sites must be complete with oxygen atoms from nitrate anions to produce a 10-coordination number (bicapped square antiprismatic), whereas four of these sites must be complete with (N) and (S) atoms from two bidentate ligands (Achar et al., 2010; Apohan et al., 2017). Since H₂O molecules are not a component of the coordination sphere, research using mass

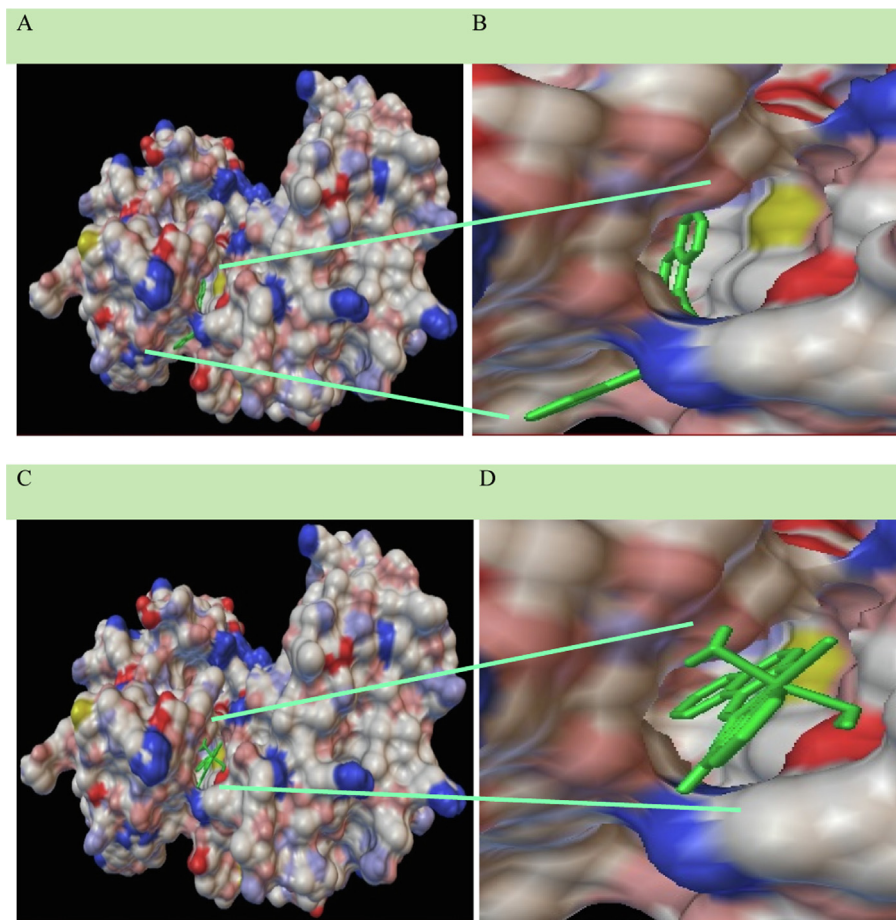


Fig. 6. (A) ERK2 structure with the docked ligand. (B) Detailed structure of the docked ligand. (C) ERK2 structure with the docked Mn(II) complex. (D) Detailed structure of the docked Mn(II) complex (Ligand and Mn(II) complex are in green).

spectroscopy, FTIR, and elemental analysis of the complexes shows that crystalline water crystallizes outside of it. To confirm the chemical structure of the ligand (L), we used ^1H NMR and ^{13}C NMR spectra, but the complexes' paramagnetic properties prevented us from doing so (Elnima et al., 1981; El-Saied et al., 2018; Ghani & Mansour, 2012).

The Cr (III) complex (2) showed four bands at 510, 440, 390, and 282 nm which indicates the electronic transitions of the type $^4\text{A}_{2g}(\text{F}) \rightarrow ^4\text{T}_{2g}(\text{F})$, $^4\text{A}_{2g}(\text{F}) \rightarrow ^4\text{T}_{1g}(\text{F})$, and $^4\text{A}_{2g}(\text{F}) \rightarrow ^4\text{T}_{1g}(\text{P})$, transitions. These bands correspond to the octahedral Cr (III) complex (Cavalcanti et al., 2004). Mn (II) complex (3) manifest also has weak absorption bands at 710, 620, and 500 nm attributed to $^6\text{A}_{1g} \rightarrow ^4\text{T}_{1g}(4p)(\square_1)$, $^6\text{A}_{1g} \rightarrow ^4\text{Eg}(4D)(\square_2)$, $^6\text{A}_{1g} \rightarrow ^4\text{Eg}(4G)(\square_3)$, and $^6\text{A}_{1g} \rightarrow ^4\text{T}_{1g}(4G)(\square_4)$, respectively. This property of Mn (II) confirms that its structure is octahedral in shape. Since the Zn (II) diamagnetic complex has a d^{10} system, it suppressed the appearance of d-d transitions. The bands that have been seen are from intraligand transitions (EL-Tabl et al., 2008).

FTIR, mass spectrometry, chemical analysis, magnetic susceptibility testing, and conductivity measurements were all employed to deduce the structure of the novel Schiff base and its complexes. All of the complexes are non-electrolytic, as determined by experiments conducted in isopropanol solutions (1.0 mM) (molar conductance between 23 and 28 $\text{Scm}^2\text{mol}^{-1}$). Complexes were completely insoluble in nonpolar solvents as compared to DMSO, methanol, isopropanol, acetone, toluene, and acetone. Due to the presence of unpaired 4f electrons that are effectively protected by 5 s₂ and 5 p₆ electrons, the magnetic moment values demonstrate that the tri-positive lanthanide ions are paramagnetic. This

suggests that mononuclear trivalence is a characteristic that all complexes share (Ermler et al., 2013; Elumalai & Hansen 2020).

EL-Tabl et al., (2008) and Ghrab et al., (2018) claim that the two bands at 1631 and 1570 cm^{-1} are members of the azomethine ($-\text{C}=\text{N}-$) group (2018). The ligands of the metal complexes (2) and (3), HL, are negatively charged and tridentate ligands composed of benzimidazole, azomethine, and a deprotonated phenolic hydroxyl group on their nitrogen atoms. Evidence for the coordination condition was provided by the absence of the characterized band to the hydroxyl group $\nu(\text{OH})$ as well as the concurrent positive change of the $(\text{C}-\text{O})$ phenolic band and the negative charge of the azomethine group $(\text{C}=\text{N})$ band. This coordination style is supported by a new summit that was granted to (O), (N), and (Cl)M, sequentially, at (685–660), (590–555), and (420–412) cm^{-1} (Gumus et al., 2003).

On the other hand, our results showed that the percentage mortality of the 4th larval stage of *Ae. aegypti* mosquito vector post-treatment with the compounds under investigation was positively correlated with the applied concentrations, however the $\text{C}_{19}\text{H}_{15}\text{N}_3\text{O}$ (H2L) have produced the highest efficacy of the larval mortality of the mosquito vector followed by the efficacy of $\text{C}_{19}\text{H}_{16}\text{Cl}_2\text{CrO}_2\text{N}_3$ then followed by the efficacy of $\text{C}_{19}\text{H}_{16}\text{ClMnO}_3\text{N}_3$ and $\text{C}_{19}\text{H}_{16}\text{ClZnO}_3\text{N}_3$ respectively. The fluctuations in the percentage mortalities obtained for the different concentrations of different compounds tested against the present mosquito larvae support this conclusion (Mahyoub, 2013; Al-Zahrani et al., 2019; Jany et al., 2002). The plant extract that demonstrated an effect on *Culex quinquefasciatus* (Iqbal et al., 2018) and the antibacterial were more efficient materials, according to a different study com-

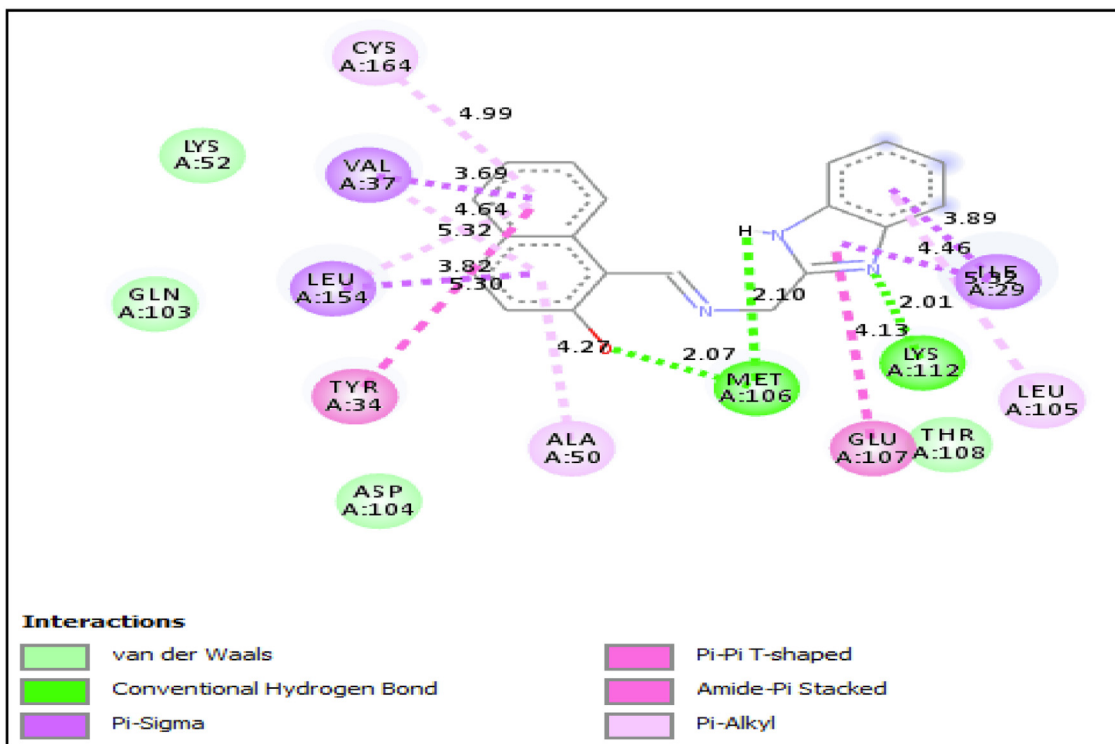


Fig. 7. The two dimensions(2D) scheme of the closest interactions between the ligand and the active site residues of ERK2.

Table 4
Bioactivities of the ligand with its metal complexes on bacteria and fungi.

Compounds	Inhibition zone in mm		
	<i>E. coli</i>	<i>B. subtilis</i>	<i>A. niger</i>
DMSO	0	0	0
Nystatin	-	-	32
Tetracycline	35	38	-
C ₁₉ H ₁₅ N ₃ O (1)	30	32	25
C ₁₉ H ₁₆ O ₂ N ₃ Cl ₂ Cr (2)	23	24	22
C ₁₉ H ₁₈ O ₃ N ₃ ClMn (3)	26	24	25
C ₁₉ H ₁₇ O ₂ N ₃ Cl ₂ Zn (4)	15	20	20

paring the larvicidal activity on *Ae. aegypti* larvae (Khalil & Mohamed, 2022). These insecticides stop the sodium channels in insects, which prolongs the time that they are open. Nerve impulses consequently continue to spread steadily. As a result, insect mortality significantly increased.

The ability of the ligand and the Mn (II) complex to bind to the ERK2 enzyme was evaluated and may contribute, at least in part, to their anticancer activity (Jeevitha et al., 2022).

5. Conclusion

A Schiff base ligand was produced by combining 2-(1H-benzo [d]imidazol-2-yl)methenamine and 2-hydroxy naphthyl aldehyde. Metal complexes were made by condensing ligands (H2L) and metal salt (ZnCl₂, CrCl₃ 6H₂O, and MnCl₂·4H₂O). The metal complexes' antibacterial and antifungal effects on *Escherichia coli* and *Bacillus subtilis* demonstrate that they exhibited promising activity, whereas *Aspergillus niger* only responded moderately. With inhibitory concentration IC₅₀ values of 6.7, 1.1, and 0.7 µg for breast adenocarcinoma cell line MCF-7, hepatocellular carcinoma cell line HepG₂, and colorectal adenocarcinoma cell line HCT 116, respectively, manganese complex was discovered to have the most toxic effects. Chromium (III) and manganese (II) complexes both exhibit

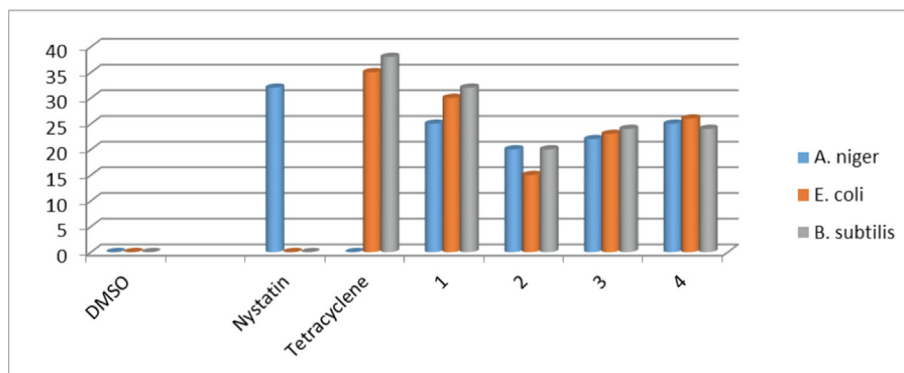


Fig. 8. Bioactivities evaluation of the ligand with its metal complexes on bacteria and fungus.

Table 5
Laboratory results an evaluation of insecticides used against the larvae of *Ae.aegypti*.

Insecticide Used	Conc. (ppm)	Mortality (%) ^a	LC ₅₀ (ppm)	Lower limit	Upper limit	Index	RR
C ₁₉ H ₁₅ N ₃ O (H ₂ L) (1)	1	19.4	2.521	1.563	3.406	100	1
	3	53.1					
	5	72.4					
	8	87.8					
	10	99.0					
C ₁₉ H ₁₆ O ₂ N ₃ Cl ₂ Cr (2)	1	15.3	3.458	2.141	4.877	72.903	1.372
	3	34.7					
	5	60.2					
	8	82.7					
	10	90.8					
C ₁₉ H ₁₈ O ₃ N ₃ ClMn (3)	1	7.1	4.764	2.868	7.34	52.918	1.89
	3	19.4					
	5	50.0					
	8	71.4					
	10	88.3					
C ₁₉ H ₁₇ O ₂ N ₃ Cl ₂ Zn (4)	1	2.0	6.965	5.381	10.018	36.195	2.763
	3	9.2					
	5	31.6					
	8	55.1					
	10	73.5					

^a Five replicates of 20 larvae.

Table 6
Calculation of LC₅₀ values for insecticides used on *Ae. aegypti* larvae.

No	Line name	LC ₅₀	Lower limit	Upper limit	Index	RR
1	C ₁₉ H ₁₅ N ₃ O (H ₂ L)	2.52	1.563	3.406	100	1
2	C ₁₉ H ₁₆ Cl ₂ CrO ₂ N ₃	3.457	2.141	4.877	72.903	1.372
3	C ₁₉ H ₁₆ ClMnO ₃ N ₃	4.779	2.868	7.34	52.918	1.89
4	C ₁₉ H ₁₆ ClZnO ₃ N ₃	6.964	5.381	10.018	36.195	2.763

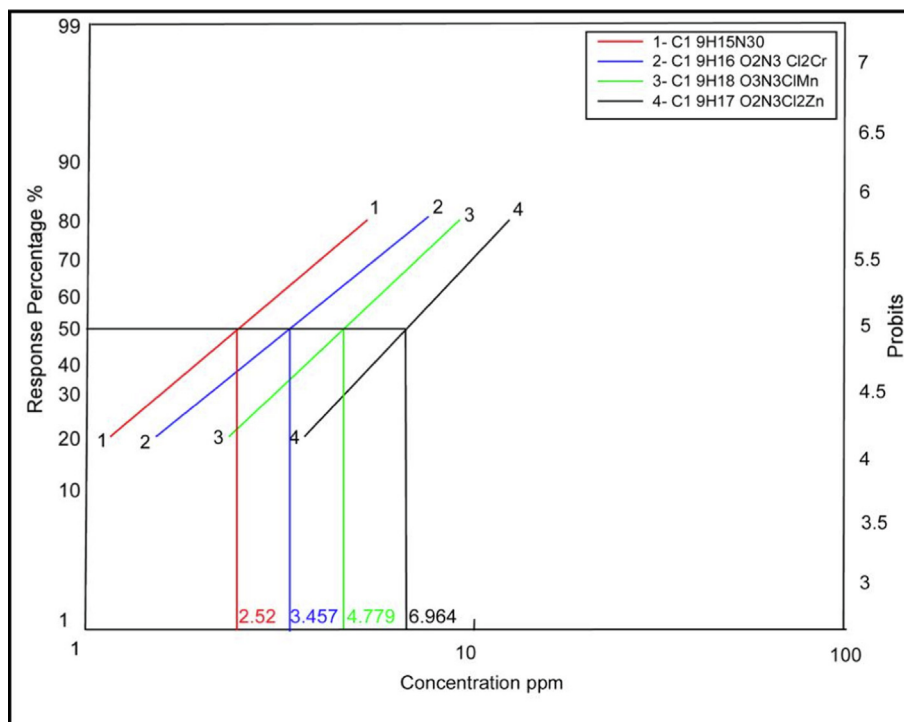


Fig. 9. Toxicity estimation of all compounds (with different concentrations) against *Ae. aegypti* using dipping bioassay techniques.

exciting toxicity against *Ae. aegypti* larvae, with lethal concentration LC₅₀ values of 3.458 and 4.764 ppm, respectively, according to the results of the complexes' bioassay study on mosquito larvae.

Declaration of Competing Interest

The authors declare that they have no known competing financial interests or personal relationships that could have appeared to influence the work reported in this paper.

Acknowledgment

This research project was funded by the Deanship of Scientific Research, Princess Nourah bint Abdulrahman University, through the Program of Research Project Funding After Publication, grant No (43- PRFA-P-44).

References

- Abdelgawad, M.A., Bakr, R.B., Omar, H.A., 2017. Design, synthesis and biological evaluation of some novel benzothiazole/benzoxazole and/or benzimidazole derivatives incorporating a pyrazole scaffold as antiproliferative agents. *Bioorganic chemistry* 74, 82–90.
- Abdelkarim, A.T., Al-Shomrani, M.M., Rayan, A.M., El-Sherif, A.A., 2015. Mixed ligand complex formation of cetrizine drug with bivalent transition metal (II) ions in the presence of 2-aminomethylbenzimidazole: synthesis, structural, biological, pH-metric and thermodynamic studies. *Journal Solution Chemistry* 44, 1673–1704.
- Achar, K.C., Hosamani, K.M., Seetharamareddy, H.R., 2010. In-vivo analgesic and anti-inflammatory activities of newly synthesized benzimidazole derivatives. *European journal of medicinal chemistry* 45 (5), 2048–2054.
- Algami G. Abdullah, Jazem A Mahyoub 2022. Efficacy of certain conventional and non-conventional insecticides against a vector of dengue fever, the *Aedes aegypti* Mosquito in Saudi Arabia. *Entomological Research*. doi: 10.1111/1748-5967.12607
- Al-Hakimi, A.N., Alminderej, F., Aroua, L., Alhag, S.K., Alfai, M.Y., Mahyoub, J.A., et al., 2020. Design, synthesis, characterization of zirconium (IV), cadmium (II) and iron (III) complexes derived from Schiff base 2-aminomethylbenzimidazole, 2-hydroxynaphthaldehyde and evaluation of their biological activity. *Arabian Journal of Chemistry* 13 (10), 7378–7389.
- Alorini, T.A., Al-Hakimi, A.N., Saeed, S.E., Alhamzi, E.H. and Albadri, A.E. 2022. Synthesis, characterization, and anticancer activity of some metal complexes with a new Schiff base ligand. *Arabian Journal of Chemistry*, 1;15(2):103559.
- Al-Zahrani Mohamd R. 1 Jazem A. Mahyoub. 1, 2, *, Al-Ghamdi Khalid M. 1 and Al-Solami Habeeb M. 2019. Bioefficacy of some insect growth regulators and plant extracts against mosquito larvae of *Aedes aegypti*. *GSC Biological and Pharmaceutical Sciences*, 2019,06(01),001 – 006.
- Apoan, E., Yilmaz, U., Yilmaz, O., Serindag, A., Kuçukbay, H., Yesilada, O., Baran, Y., 2017. Synthesis, cytotoxic and antimicrobial activities of novel cobalt and zinc complexes of benzimidazole derivatives. *Journal of Organometallic Chemistry* 828, 52–58.
- Bansal, Y., Silakari, O., 2012. The therapeutic journey of benzimidazoles: A review. *Bioorganic & medicinal chemistry* 20 (21), 6208–6236.
- Biovia, D.S., 2015. Discovery studio visualizer v16. 1.0, 15350.
- Cavalcanti, E.S.B., Morais, S.M.D., Lima, M.A.A., Santana, E.W.P., 2004. Larvicidal activity of essential oils from Brazilian plants against *Aedes aegypti* L. *Memórias do Instituto Oswaldo Cruz* 99, 541–544.
- Cavicchioli, M., Zaballa, A.M.L., Paula, Q.A.D., Prieto, M.B., Oliveira, C.C., Civitareale, P., et al., 2019. Oxidative assets toward biomolecules and cytotoxicity of new oxindolimine-copper (II) and zinc (II) complexes. *Inorganics* 7 (2), 12.
- Cheddie, A., Shintre, S.A., Bantho, A., Mockett, C., Koorbanally, N.A., 2020. Synthesis and antibacterial activity of a series of 2-trifluoromethylbenzimidazole-thiazolidinone derivatives. *Journal of Heterocyclic Chemistry* 57 (1), 299–307.
- Collee, J.G., Mackie, T.J., McCartney, J.E., 1997. *Practical Medical Microbiology*. Churchill Livingstone, New York, p. 978.
- Djemoui, A., Naouri, A., Ouahrani, M.R., Djemoui, D., Lahcene, S., Lahrech, M.B., et al., 2020. A step-by-step synthesis of triazole-benzimidazole-chalcone hybrids: Anticancer activity in human cells+. *Journal of Molecular Structure* 1204, 127487.
- Dokla, E.M., Abutaleb, N.S., Milik, S.N., Li, D., El-Baz, K., Shalaby, M.A.W., et al., 2020. Development of benzimidazole-based derivatives as antimicrobial agents and their synergistic effect with colistin against gram-negative bacteria. *European Journal of Medicinal Chemistry* 186, 111850.
- Elinima, E.I., Zubair, M.U., Al-Badr, A.A., 1981. Antibacterial and antifungal activities of benzimidazole and benzoxazole derivatives. *Antimicrobial agents and chemotherapy* 19 (1), 29–32.
- El-Saied, F.A., Salem, T.A., Shakkofa, M.M., Al-Hakimi, A.N., 2018. Anti-neurotoxic evaluation of synthetic and characterized metal complexes of thiosemicarbazone derivatives. *Applied Organometallic Chemistry* 32 (4), e4215.
- El-Sherif, A.A., 2011. Synthesis and characterization of some potential antitumor palladium (II) complexes of 2-aminomethylbenzimidazole and amino acids. *Journal of Coordination Chemistry* 64 (12), 2035–2055.
- El-Tabl, A.S., El-Saied, F.A., Plass, W., Al-Hakimi, A.N., 2008. Synthesis, spectroscopic characterization and biological activity of the metal complexes of the Schiff base derived from phenylaminoacetohydrazide and dibenzoylmethane. *Spectrochimica Acta Part A: Molecular and Biomolecular Spectroscopy* 71 (1), 90–99.
- Elumalai, V., Hansen, J.H., 2020. A green, scalable, one-minute synthesis of benzimidazoles. *Synlett* 31 (06), 547–552.
- Ermler, S., Scholze, M., Kortenkamp, A., 2013. Seven benzimidazole pesticides combined at sub-threshold levels induce micronuclei in vitro. *Mutagenesis* 28 (4), 417–426.
- Frisch, M.J., Trucks, G.W., Schlegel, H.B., Scuseria, G.E., Robb, M.A., Cheeseman, J.R., Montgomery J.A., Jr, T.K.K.N., Vreven, K.N., Kudin, J.C., & Burant, J.M. 2013. Millam, Gaussian 09, Revision D.01, Gaussian, Inc., Wallingford CT.
- Ganie, A.M., Dar, A.M., Khan, F.A., Dar, B.A., 2019. Benzimidazole derivatives as potential antimicrobial and antiulcer agents: A mini review. *Mini reviews in medicinal chemistry* 19 (16), 1292–1297.
- Ghani, N.T.A., Mansour, A.M., 2012. Novel palladium (II) and platinum (II) complexes with 1H-benzimidazol-2-ylmethyl-N-(4-bromo-phenyl)-amine: Structural studies and anticancer activity. *European journal of medicinal chemistry* 47, 399–411.
- Ghrab, S., Aroua, L., Mekni, N., Beji, M., 2018. Simple approach for the regioselective synthesis of a bis (β-aminoalcohol) derived from polyoxyethylene: first report of fast ring-opening of polyoxyethylene diglycidyl ethers with sodium amide. *Research on Chemical Intermediates* 44 (5), 3537–3548.
- Gumuş, F., Algul, O., Eren, G., Eroglu, H., Diril, N., Gur, S., Ozkul, A., 2003. Synthesis, cytotoxic activity on MCF-7 cell line and mutagenic activity of platinum (II) complexes with 2-substituted benzimidazole ligands. *European journal of medicinal chemistry* 38 (5), 473–480.
- Hayat S. Al-Rashidi, Wafa Mohammed Al-Otaibi, Khalid Mohammed Alghamdi, Jazem A. Mahyoub, 2022. Seagrasses extracts as potential mosquito larvicides in Saudi Arabia. *Saudi Journal of Biological Sciences*. Volume 29, Issue 12, December 2022, 103433.
- Huszar, S., Chibale, K., Singh, V., 2020. The quest for the holy grail: new antitubercular chemical entities, targets and strategies. *Drug Discovery Today* 25 (4), 772–780.
- Ibrahim, S.R., Abdallah, H.M., Mohamed, G.A., Ross, S.A., 2016. Integracides HJ: New tetracyclic triterpenoids from the endophytic fungus *Fusarium* sp. *Fitoterapia* 112, 161–167.
- Iqbal, J., Ishtiaq, F., Alqarni, A.S., Owayss, A.A., 2018. Evaluation of larvicidal efficacy of indigenous plant extracts against *Culex quinquefasciatus* (Say) under laboratory conditions. *Turkish Journal of Agriculture and Forestry* 42 (3), 207–215.
- Jeevitha R. J., Mary Imelda Jayaseeli, A., Sankarganesh, M., & Nandini Asha, R. 2022. Bovine serum albumin interaction, molecular docking, anticancer and antimicrobial activities of Co (II) Schiff base complex derived from Nophen ligand. *Journal of Biomolecular Structure and Dynamics*, 1-9.
- Khalil, E.A., Mohamed, G.G., 2022. Preparation, spectroscopic characterization and antitumor-antimicrobial studies of some Schiff base transition and inner transition mixed ligand complexes. *Journal of Molecular Structure* 1249, 131612.
- Li, Y. F., Wang, G. F., Luo, Y., Huang, W. G., Tang, W., Feng, C. L., Shi, L.P., Ren, Y.D., Zuo, J.P. & Lu, W. 2007. Identification of 1-isopropylsulfonyl-2-amine benzimidazoles as a new class of inhibitors of hepatitis B virus. *European journal of medicinal chemistry*, 42(11–12), 1358–1364.
- Mahmoud, A.M., Al-Abd, A.M., Lightfoot, D.A., El-Shemy, H.A., 2012. Anti-cancer characteristics of mevinolin against three different solid tumor cell lines was not solely p53-dependent. *Journal of enzyme inhibition and medicinal chemistry* 27 (5), 673–679.
- Mahyoub, J.A., 2019. Biological effects of synthesized silver nanoparticles using *Dodonaea viscosa* leaf extract against *Aedes aegypti* (Diptera: Culicidae). *Journal of Entomology and Zoology Studies* 7 (1), 827–832.
- Jazem A. Mahyoub, 2013. Evaluation of the IGRs alstynin and pyriproxyfen as well as the plant extract jojoba oil against the mosquito *Aedes aegypti*. *J. OF Pure and Applied Microbiology* 1, December. Vol. (07), NO (04).
- Morris, G.M., Huey, R., Olson, A.J., 2008. Using autodock for ligand-receptor docking. *Current protocols in bioinformatics* 24 (1), 8–14.
- Naema, H.Y., Hoda, A.E., Mohamed, G., 2017. Synthesis, spectroscopic and DNA binding ability of Co(II), Ni(II), Cu(II) and Zn(II) complexes of Schiff base ligand (E)-1-(((1H-benzod[imidazol-2-yl)methylimino) methyl)naphthalen-2-ol. X-ray crystal structure determination of cobalt (II) complex. *Materials Science and Engineering: C* 75, 1059–1067.
- Narasimhan, B., Sharma, D., Kumar, P., 2012. Benzimidazole: a medicinally important heterocyclic moiety. *Medicinal Chemistry Research* 21 (3), 269–283.
- Patel, V.M., Patel, N.B., Chan-Bacab, M.J., Rivera, G., 2020. N-Mannich bases of benzimidazole as a potent antitubercular and antiprotozoal agents: Their synthesis and computational studies. *Synthetic Communications* 50 (6), 858–878.
- Rahuman, A.A., Gopalakrishnan, G., Ghouse, B.S., Arumugam, S., Himalayan, B., 2000. Effect of *Feronia limonia* on mosquito larvae. *Fitoterapia* 71 (5), 553–555.
- Shakkofa, M.M., Morsy, N.A., Rasras, A.J., Al-Hakimi, A.N., Shakkofa, A.M., 2021. Synthesis, characterization, and density functional theory studies of

- hydrazone–oxime ligand derived from 2, 4, 6-trichlorophenyl hydrazine and its metal complexes searching for new antimicrobial drugs. *Applied Organometallic Chemistry* 35 (2), e6111.
- Sondhi, S.M., Singh, N., Kumar, A., Lozach, O., Meijer, L., 2006. Synthesis, anti-inflammatory, analgesic and kinase (CDK-1, CDK-5 and GSK-3) inhibition activity evaluation of benzimidazole/benzoxazole derivatives and some Schiff's bases. *Bioorganic & medicinal chemistry* 14 (11), 3758–3765.
- Wang, X.J., Xi, M.Y., Fu, J.H., Zhang, F.R., Cheng, G.F., You, Q.D., 2012. Synthesis, biological evaluation and SAR studies of benzimidazole derivatives as H1-antihistamine agents. *Chinese Chemical Letters* 23 (6), 707–710.
- Welsh, A., Rylands, L.I., Arion, V.B., Prince, S., Smith, G.S., 2020. Synthesis and antiproliferative activity of benzimidazole-based, trinuclear neutral cyclometallated and cationic, N[^] N-chelated ruthenium (ii) complexes. *Dalton Transactions* 49 (4), 1143–1156.
- Yılmaz, U., Kuçukbay, H., 2020. Synthesis and spectral characterization of new benzimidazolium compounds containing sulfur. *Phosphorus, Sulfur, and Silicon and the Related Elements* 195 (7), 580–585.
- Zhou, S., Huang, G., 2020. Synthesis of anti-allergic drugs. *RSC advances* 10 (10), 5874–5885.

Further Reading

- World Health Organization (WHO). 1996. Report of the WHO Informal Consultation on the“ Evaluation and Testing of Insecticides”, WHO/HQ, Geneva, 7 to 11 October 1996 (No. CTD/WHOPES/IC/96.1). World Health Organization.